Evaluating CONOPS for GEO Spacecraft Identification and Custody from Non-SSA Architectures in LEO

Kevin Brannick
Raytheon Intelligence & Space

Karen Galang **Scott Reed**
Raytheon Intelligence & Space

ABSTRACT

The Space Development Agency (SDA) proposes a future National Defense Space Architecture (NDSA) that features multiple layers in low Earth orbit (LEO), each with a unique mission and a potentially large number of satellites. While these systems may be required to provide a particular military capability at all times, there will likely be periods when certain satellites and sensors are not needed for a constellation to reliably and accurately provide its primary service. These redundant space assets can perform a secondary mission such as observing Resident Space Objects (RSOs) at or near geosynchronous earth orbit (GEO), effectively augmenting the Space Surveillance Network (SSN) and enhancing space domain awareness. Leveraging these efficiencies could enhance the utility of a large, resilient space architecture and also reduce costs for the government to develop and field separate space situational awareness (SSA) capabilities. The NDSA includes a Tracking Layer with a primary mission to track and target advanced missile threats and provide critical indications and warning. This paper presents the operational benefits of adding a secondary SSA mission to this Tracking Layer. Just as evolving missile threats necessitate space-based observations of the Earth, evolving space threats demand improved and persistent SSA to facilitate space asset protection. Exploiting the mission architecture's persistent access to RSO and missile observations, and the dual application of the same sensors, could potentially yield a multi-mission system at reduced cost to the government with no noticeable degradation in primary mission service to the end-users.

A notional Tracking Layer could feature spacecraft equipped with visible and/or infrared optical sensors used for Earth-pointing observations. The same sensors can produce observations of space objects when pointed away from Earth and into deep space. This function could help maintain and update an existing space catalog of RSOs and even reveal the intent and characteristics of spacecraft based on their positioning and movement over time. This paper demonstrates the feasibility and practicality of using one common proliferated LEO (pLEO) space architecture for both purposes. We model both missions with one constellation representative of a notional Tracking Layer architecture. Each spacecraft features a visible electro-optical (EO) sensor modeled after Canada's Sapphire satellite in LEO, which provides RSO observations to the SSN. Actual cataloged information of RSOs, including publicly available ephemeris and object size parameters, enable simulations of RSO detections, yielding the quantity of space objects observed and revisit rates. We examine the quality of orbits determined from the aggregated RSO observations and assess the effectiveness of the space surveillance mission. We evaluate these metrics over several time periods of availability for the secondary mission and identify concepts of operations (CONOPS) that represent the different duty cycles, while ensuring that the primary mission requirements are not compromised, or at most have minimal impacts.

1. INTRODUCTION

Several future military space architectures will be designed to address modern advances in foreign missile technology. Defense organizations such as the Space Development Agency (SDA), Missile Defense Agency (MDA), and Defense Advanced Research Projects Agency (DARPA), are all exploring resilient space-based concepts to identify and persistently track hypersonic weapons. The SDA's notional Tracking Layer constellation, for example, features a large, proliferated set of satellites in low Earth orbit (LEO) to provide indications and warning of global missile activity and enable continuous custody of hypersonic glide vehicles (HGVs). While the primary mission for these space systems is missile warning and tracking, there will likely be significant down time with no active missiles in some or all geographic regions. This presents an opportunity for a secondary mission to piggyback on the constellation and share time, sensors, and/or the satellite bus with the primary mission.

SDA outlines six other critical priorities for space and proposes a National Defense Space Architecture (NDSA) with unique "layers", or constellations, of satellites to service each of them [1]. One important aspect of space security not covered by the NDSA is the monitoring of resident space objects (RSOs) at or near geosynchronous Earth orbit (GEO), including adversarial military and intelligence satellites. The Space Surveillance Network (SSN) currently identifies and tracks a large share of RSOs at GEO. It features ground-based sensors like the Ground-Based Electro-Optical Deep Space Surveillance (GEODSS) system and space-based sensors like Canada's electro-optical (EO) Sapphire satellite in LEO, which contributes visible-band metric observations of RSOs. These systems' data combine with other sensor and collateral information for robust space domain awareness necessary for civil, commercial, and national security space operations.

Ground systems like GEODSS have larger apertures than space-based surveillance systems, allowing for higher detection sensitivity near GEO. This enhances their ability to detect smaller objects and a larger portion of the space catalog. However, their performance may be limited by weather, daylight, and geographic location. LEO systems are unaffected by weather, but can suffer from Earth blockage, which considerably hinders performance, especially when only one satellite comprises a system, such as with Sapphire. Applying a Sapphire-like sensor to a proliferated LEO (pLEO) space architecture, such as the Tracking Layer, can potentially overcome this problem. This concept enables frequent access to the entire GEO belt and enables observation of RSOs that are outside the field of regard (FoR) of ground systems like GEODSS. Sapphire's sensor is limited in aperture size and therefore less sensitive to observing RSOs at GEO. However the intent of the system is not to resolve the structure and features of RSOs but rather to confirm the presence of newly launched satellites, contribute metric tracks to the SSN, and increase safety of flight for near Earth space missions. Alarming behavior at GEO includes foreign satellites rendezvousing with commercial satellites, decommission and recommissioning of communication satellites, and erratic movement indicative of anomalies like outgassing or unplanned component malfunction, among other things. Not all unusual behavior is threatening, but should be closely monitored for accurate and timely situational awareness.

MDA has noted the Space Tracking and Surveillance System (STSS) may include adjunct missions such as tracking on-orbit satellites [2], lending credibility to adding a secondary space situational awareness (SSA) mission to a Sapphire-like pLEO constellation. Determining the appropriate concept of operations (CONOPS) balances the capability of the secondary mission with the performance requirements of the primary mission. Both missions share persistent, simultaneous line of sight access to their targets, and can also share common sensor technology including the optical train. Several time and resource sharing plans can be derived to design a multi-mission system based on one common space architecture. It may also be possible to perform both missions on the same platform independently and simultaneously. Either way, this concept presents an option for the government to augment the SSN and provide an additional layer of utility to the NDSA. It can also result in an overall reduction in spending by eliminating the need for additional, separate space surveillance systems.

2. PAYLOAD & MISSION MODELING

The first of two main objectives of this study is to develop CONOPS for space surveillance of GEO from a pLEO system. The second objective, discussed in Section 5, is to evaluate the utility of the RSO observations in determining orbits. We take a physics-based modeling approach to simulate the metric tracking performance of Sapphire-class EO sensors on a notional Tracking Layer constellation. Analysis includes geometric field of view (FoV) analysis and sensor detection performance. This process is repeated for several different periods of availability over the mission. Each unique availability, or duty cycle, for the space surveillance mission corresponds to a CONOP indicating whether the primary and secondary missions can be performed simultaneously and if they could share a common sensor.

We modeled the Tracking Layer architecture with 15 satellites uniformly phased on each of 10 evenly distributed planes. Each orbital plane is inclined 70°, and each satellite is at an altitude of 1,000 km. This design enables global, stereo coverage of advanced missile systems via medium field of view infrared sensors. Each satellite includes a visible EO sensor modeled after Canada's Sapphire satellite payload in LEO. To simulate the performance of the space surveillance mission, each sensor is placed on the zenith-deck of the spacecraft to point toward deep-space. We chose Sapphire as the representative system for this study because many of its design and performance characteristics are publicly available, and its aperture size is approximately the geometric mean of both the smallest and largest apertures expected for this type of mission.

We developed an EO model of the Sapphire payload that calculates the signal-to-noise ratio (SNR) of the collected energy at the detector level, and assumed the sensor can detect RSOs with relative visual magnitude of 15 [3]. The focal plane array (FPA) size, output, and noise characteristics are modeled after a commercially available back illuminated charge-couple device (CCD) [4]. Tbl. 1 shows several key design parameters of the sensor design. The sensor's ground sample distance (GSD) indicates each pixel covers about one kilometer of the GEO belt. This is a limiting factor in resolving multiple RSOs near each other. Constraining the integration time to 0.1 seconds ensures that the collected signals don't smear across pixels due to the relative motion of the RSOs.

Tbl 1. Sapphire-Like Sensor Parameters

Parameter	Unit	Value
Aperture diameter	cm	15
F-number	-	3.66
Field of View	deg	1.4 x 1.4
Spectral Band Cut-on Wavelength	μm	0.3
Spectral Band Cut-off Wavelength	μm	0.9
Detector pitch	μm	13
Integration Time	s	0.1000
Coadds	-	10
Well Capacity	e-	100,000
Dark Current Density	A/cm^2	1.4e-10
Read Noise	e-	2
Quantum Efficiency	-	0.9
FPA Number of Detectors X	-	1024
FPA Number of Detectors Y	-	1024
Ground Sample Distance (GSD)	km	0.95
Angular Measurement Uncertainty 1σ	arcsec	2

We used probability-of-detection (Pd) as the primary driver of sensor performance. Setting the Pd requirement to approximately 90% and a false-alarm-rate (FAR) tolerance to 1E-04 yields a necessary SNR of 6 to detect RSOs at GEO, given an integration time of 0.1 seconds [5]. We tuned the sensor design parameters such that RSOs with visual magnitude 15 register an SNR of 6 at the detectors, at 40,000 km distance. Solar phase angles were excluded below 30° and above 150°, where the solar phase angle is measured between the GEO-LEO and GEO-Sun vectors. This accounts for both stray sunlight directly entering the sensor and potential RSO eclipses.

To accurately assess energy arriving at the sensors, we modeled 448 GEO RSOs from a catalog of publicly available ephemerides and accompanying size data [6]. Each RSO is assumed to be a diffuse sphere with reflectivity of 15% [7]. Each object's cross-sectional area and reflectivity, combined with solar phase angle and range, determine the amount of solar energy reflected to each sensor in LEO. The minimum detectable target (MDT), or smallest RSO, is expressed as a function of solar phase angle in Fig. 1. The best geometric lighting conditions yield observations of 1.1 m objects. However, each satellite will encounter a range of solar phase angles that will effectively change the size of the MDT throughout the mission. The sensor is assumed to be inoperable at solar phase angles less than 30° and greater than 150°.

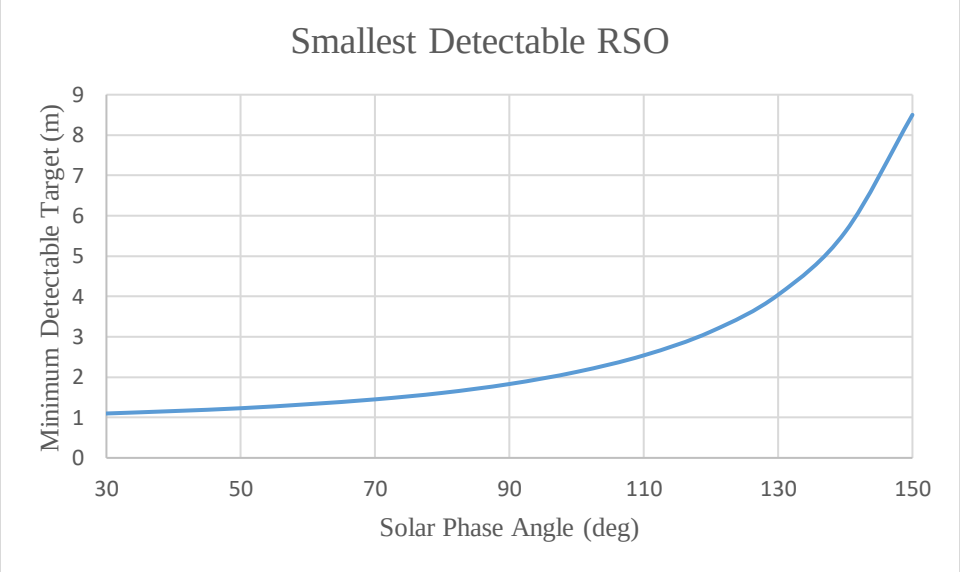

Fig. 1. Smallest Detectable RSO vs Solar Phase Angle

3. MISSION SIMULATION

The mission architecture is shown in Fig. 2, where the 448 RSOs are in blue, the 150 LEO satellites are the dots closest to Earth, and the pink lines show the sensor access from one satellite to the GEO belt. The distribution of RSO sizes is shown in Fig. 3. Approximately 14% of the objects are too small for our sensor to detect. Fig. 4 depicts the projection of the sensor's 1.4° x 1.4° FoV at GEO, with an RSO centered in view. We implemented a relatively simple pointing scheme, where each sensor boresights to 0° latitude and the same longitude as its host satellite, at a range of 40,000 km. Some RSOs never enter the sensor's FoV due to both their inclination and our sensor pointing scheme. For example, the two RSOs in the bottom left of Fig. 4 are never detected.

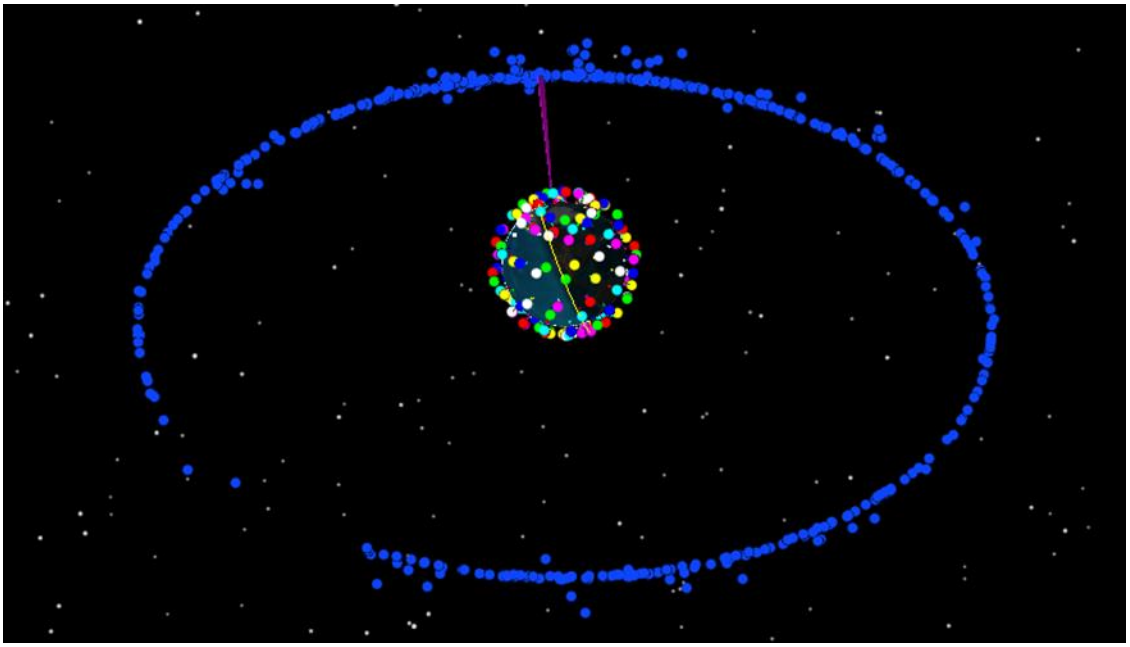

Fig. 2. Space Surveillance Mission Modeling. Image via Systems Tool Kit (STK)

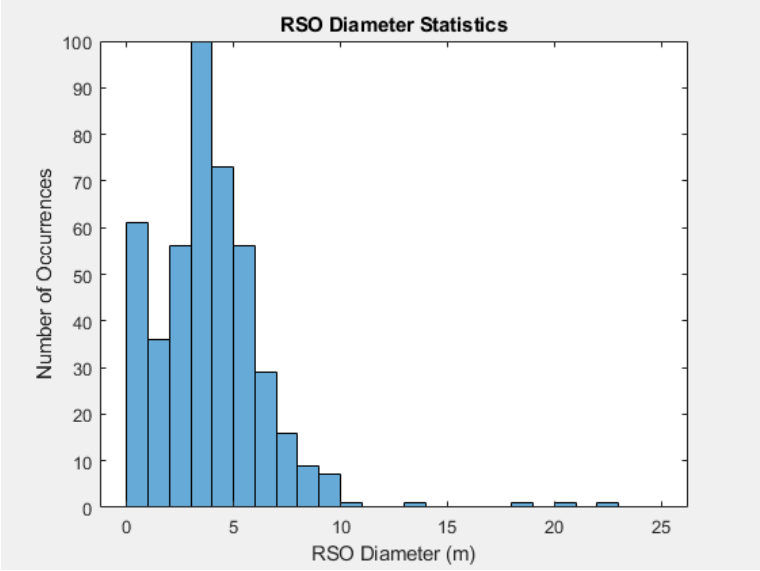

Fig. 3. Distribution of RSO Size

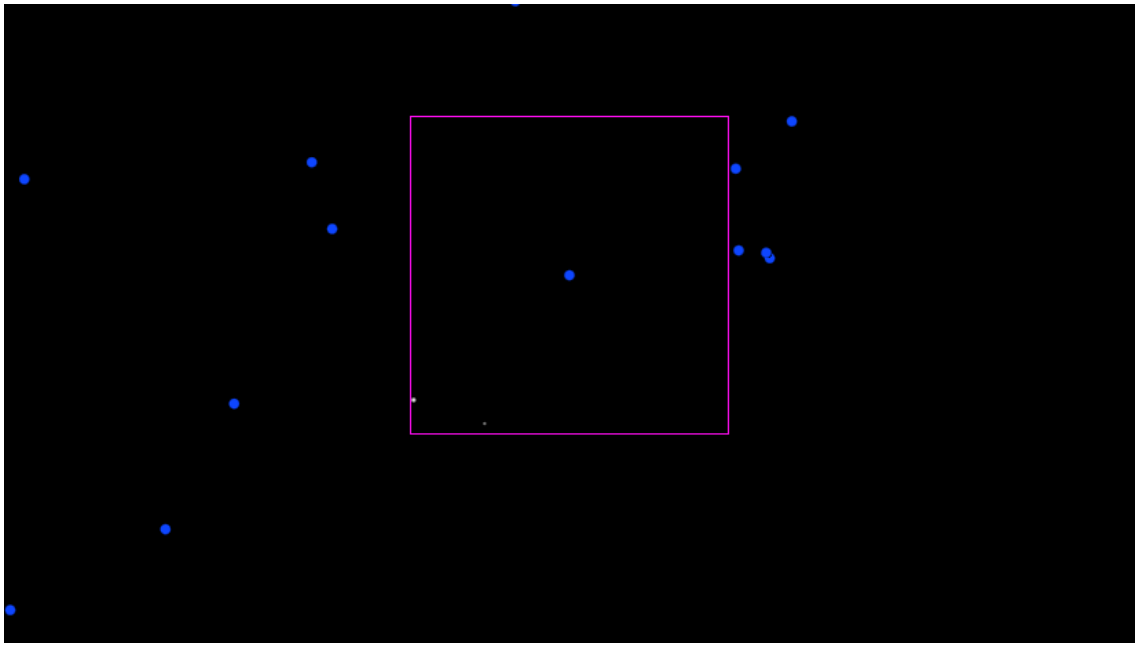

Fig. 4. Sensor FoV at GEO. Image via STK.

To capture sensor performance metrics we took a snapshot of the RSOs and then propagated the LEO satellite orbits for 24 hours on the Vernal Equinox. RSO detections were measured once every 10 seconds. We repeated this process over four different duty cycles, where 100% duty cycle means one complete period of orbit: 100%, 80%, 44%, and 34%.

100% Duty Cycle

This use case represents a dedicated sensor to the secondary mission, available during the full orbit. This would likely be a 2-axis gimbaled sensor on the zenith-deck of the spacecraft. If momentum or jitter can be mitigated to not impair the primary mission, then the secondary mission can occur while the primary mission takes place. Otherwise, the space surveillance mission can only occur when the primary is not active.

Of the 448 RSOs on-orbit, 11% (49) never enter the FoV of any sensor. These are either too high or low in latitude. Of the 399 RSOs that enter the FoV, 85% (338) are observable. 91% (55) of the 61 unobservable RSOs are caused by unfavorable solar phase angle. Fig. 5 shows that most of the 338 observable RSOs are observed up to 200 times in 24 hours. Fig. 6 shows that RSOs of similar sizes are observed over a wide range of occurrences. This may be due to wide variations in the solar phase angle during detection events. Fig. 7 shows the minimum and maximum RSO revisit times. Most RSOs experience a minimum revisit rate less than one minute and a maximum revisit rate of about eight hours. The lowest revisit rate recorded is 10 seconds and max is 17 hours. Our sample rate for detections is 10 seconds, so it could be possible that the lowest revisit rate is less than 10 seconds.

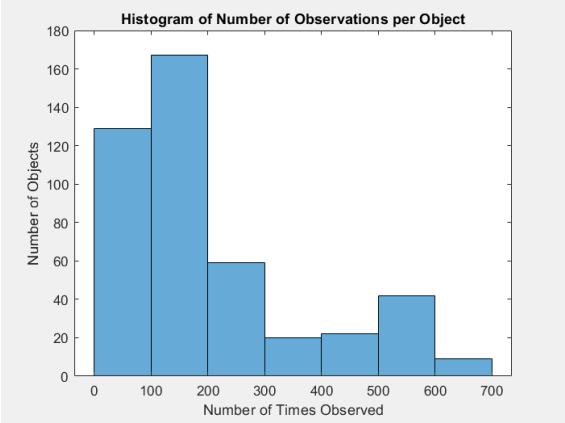

Fig. 5. Observations per RSO for 100% duty cycle.

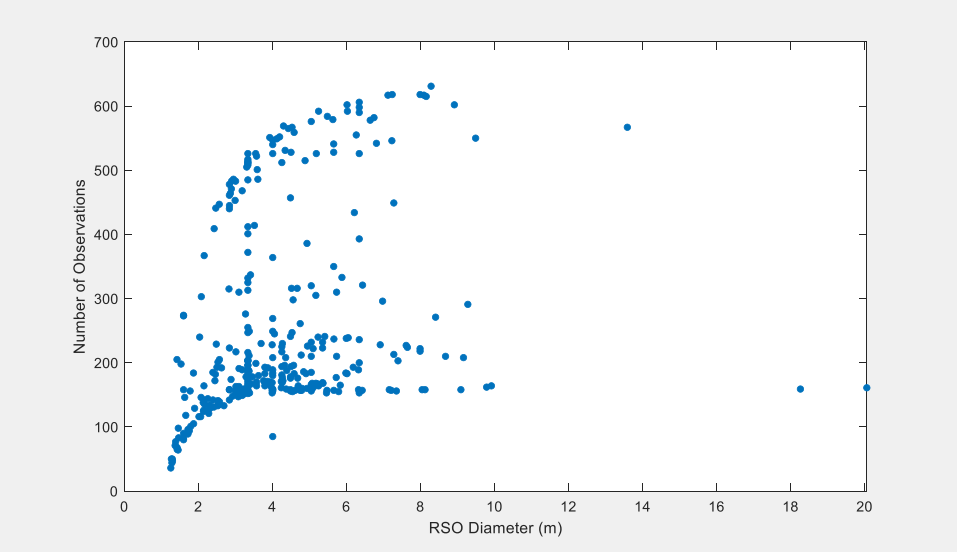

Fig. 6. Number of Observations vs RSO Size for 100% duty cycle

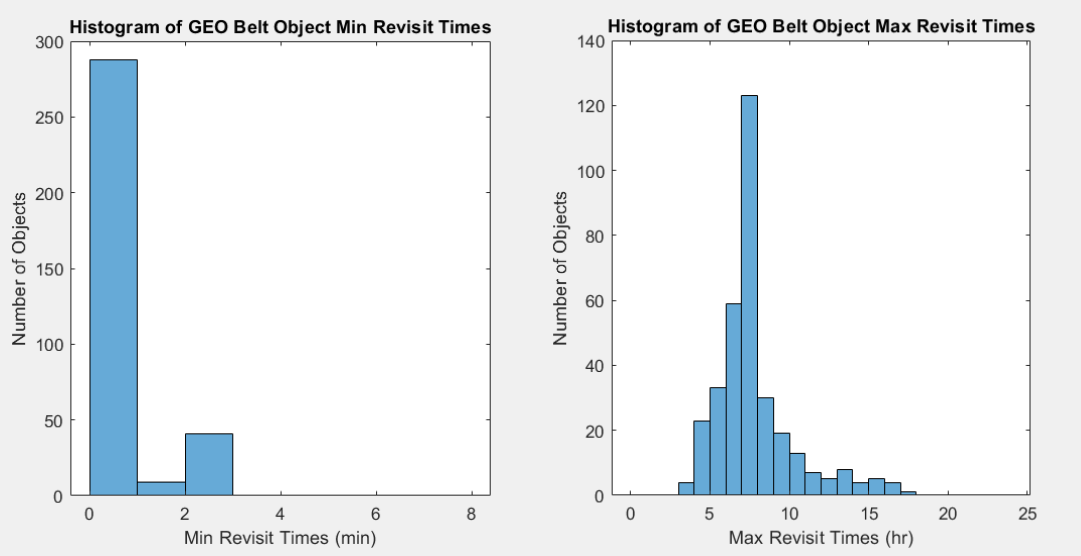

Fig 7. Min and Max Revisit Times for 100% duty cycle

80% Duty Cycle

This use case is similar to the previous, but we removed 10% duty cycle near both poles to account for any spacecraft maintenance such as attitude adjustments or sensor slewing.

Of the 448 RSOs on-orbit, 11% (50) never enter the FoV of any sensor. These are either too high or low in latitude. Of the 398 RSOs that enter the FoV, 85% (337) are observable, just one less than the 100% duty cycle case. The majority of the 61 unobservable RSOs are likely not detected due to unfavorable solar phase angles. Fig. 8 shows that most of the 337 observable RSOs are observed less than 50 or between 150 and 200 times over 24 hours. Fig. 9 shows the minimum and maximum RSO revisit times. Most RSOs experience a minimum revisit rate less than one minute and a maximum revisit rate of about eight hours. The lowest revisit rate recorded is 10 seconds and max is 17 hours.

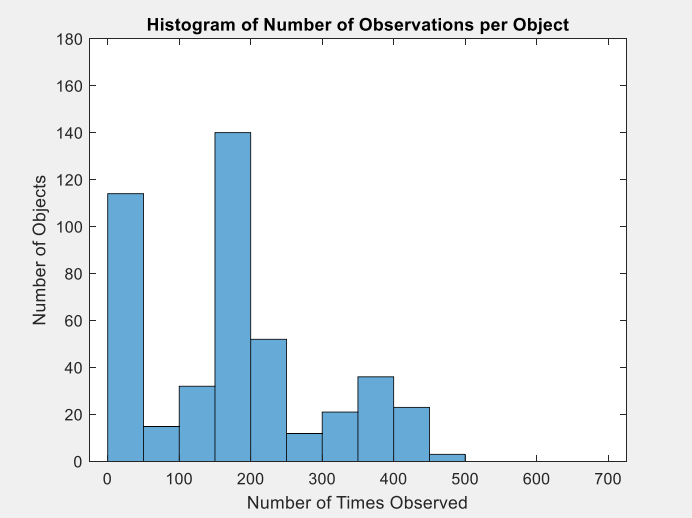

Fig. 8. Observations per RSO for 80% duty cycle

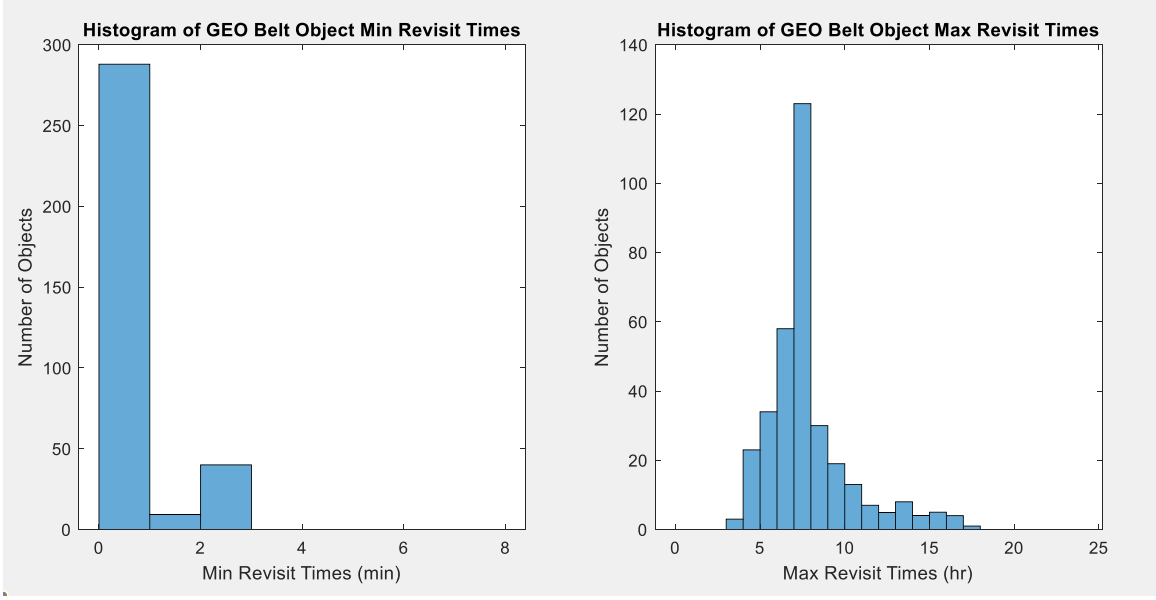

Fig. 9. Min and Max Revisit Times for 80% duty cycle

44% Duty Cycle

For this use case, we estimate that the secondary mission will only be available at latitudes below 10° south. This CONOP prioritizes notional HGV tracking missions in the Northern Hemisphere, with an additional margin just below the equator. The secondary mission could then use the same optical sensor as the primary mission on a part-time basis. Alternatively, each spacecraft could have a body-mounted sensor dedicated to the secondary mission that is available during the full orbit. However, in either case the space vehicles must be slewed to point the sensor at GEO.

Of the 448 RSOs on-orbit, 16% (70) never enter the FoV of any sensor. These are either too high or low in latitude. Of the 378 RSOs that enter the FoV, 85% (320) are observable. The majority of the 58 unobservable RSOs are likely not detected due to unfavorable solar phase angles. Fig. 10 shows that most of the 320 observable RSOs are observed up to 50 times over 24 hours. Fig. 11 shows the minimum and maximum RSO revisit times. Most RSOs experience a minimum revisit rate either less than one minute or between five and six minutes, but the most common maximum revisit rate remains at about eight hours. The lowest revisit rate recorded is 10 seconds and max is 17 hours, the same as the 100% and 80% duty cycle cases.

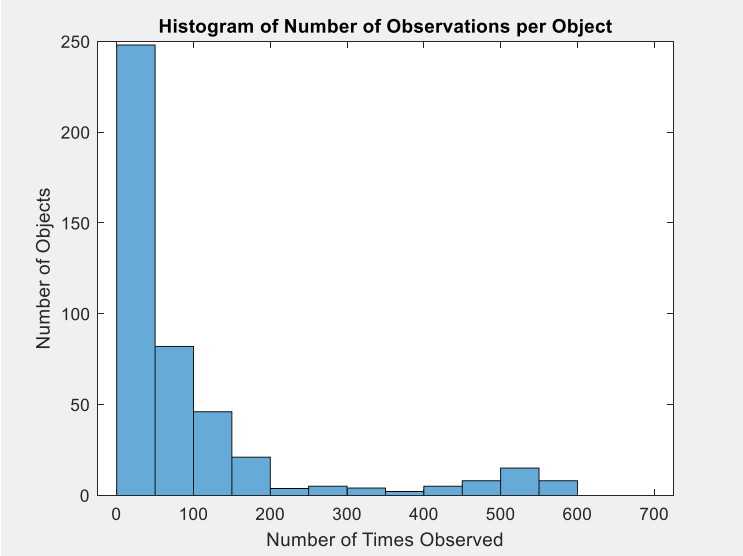

Fig 10. Observations per RSO for 44% duty cycle

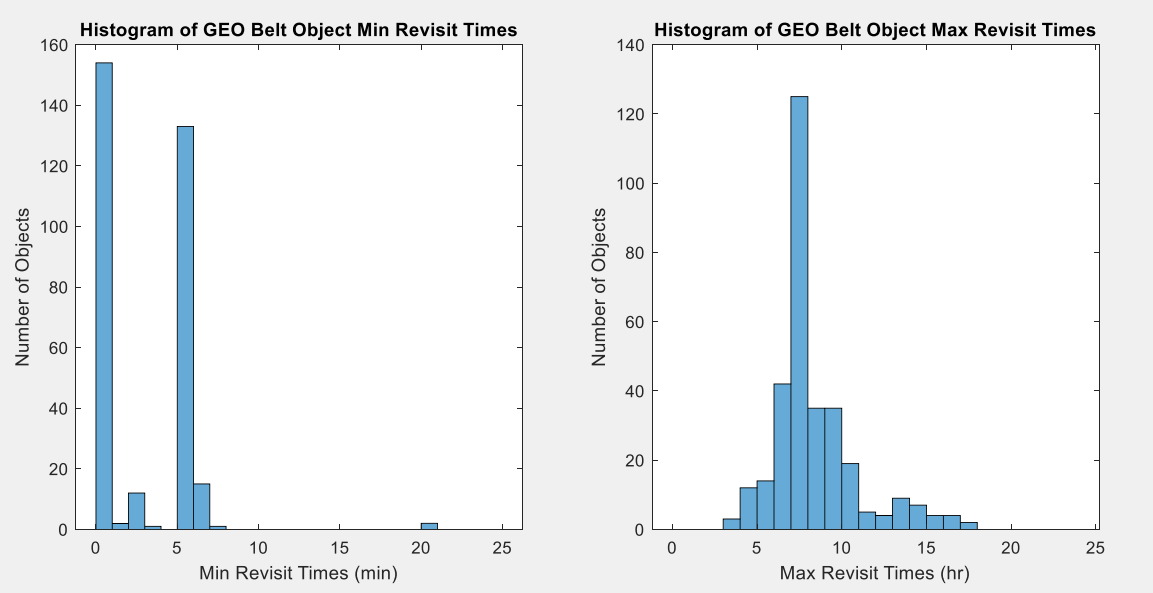

Fig. 11. Min and Max Revisit Times for 44% duty cycle

34% Duty Cycle

This use case is similar to the previous, but we removed 10% duty cycle near the South Pole to account for any spacecraft maintenance such as attitude adjustments or sensor slewing.

Of the 448 RSOs on-orbit, 16% (70) never enter the FoV of any sensor. These are either too high or low in latitude. Of the 378 RSOs that enter the FoV, 85% (320) are observable. These are the same results as the 44% duty cycle case. The majority of the 58 unobservable RSOs are likely not detected due to unfavorable solar phase angles. Fig. 12 shows that most of the 320 observable RSOs are observed up to 50 times over 24 hours. Fig. 13 shows the minimum and maximum RSO revisit times. Most RSOs experience a minimum revisit rate either less than one minute or between five and six minutes, but the most common maximum revisit rate remains at about eight hours. These are also the same results as the 44% duty cycle case. The lowest revisit rate recorded is 10 seconds and max is 17 hours, the same as the 100%, 80%, and 44% duty cycle cases.

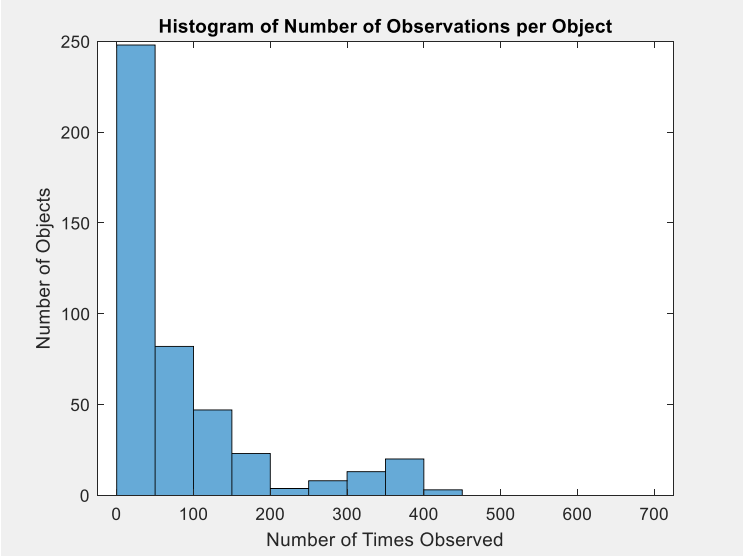

Fig. 12. Observations per RSO for 34% duty cycle

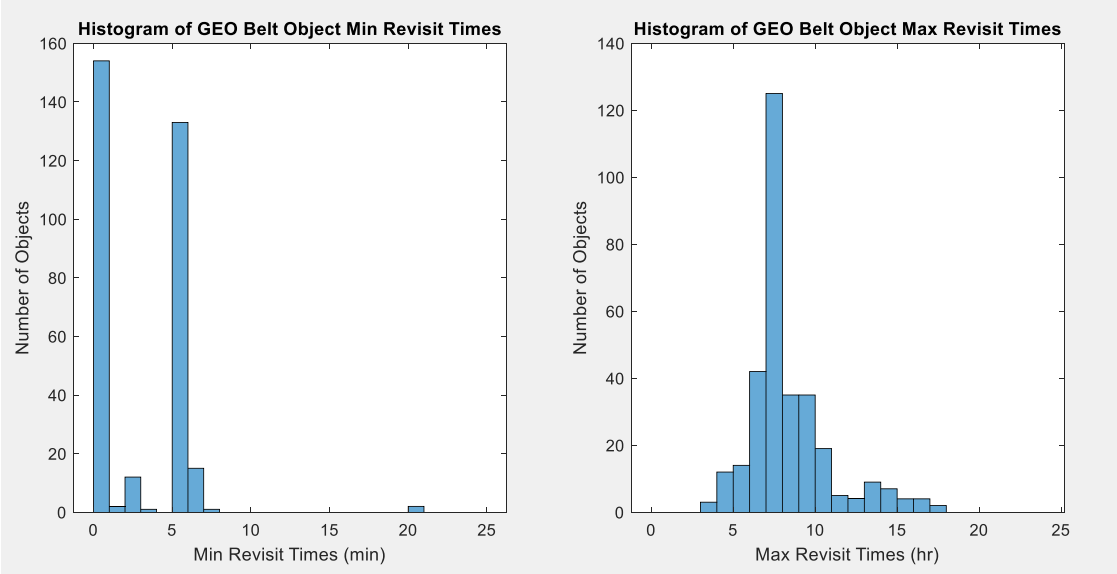

Fig. 13. Min and Max Revisit Times for 34% duty cycle

Combined Perspective

The 100% and 80% duty cycle cases each produced radiometric observations of about 75% of the total 448 cataloged GEO RSOs. The 44% and 34% duty cycle cases each produce observations of about 71% of the objects. Each duty cycle case took 17 hours to detect all of the RSOs it could observe, as shown in Fig. 14. Note that the yellow 44% curve is masked by the purple 34% curve. Although the 100% and 80% cases observed about the same number of RSOs, the 100% case produced 13% more total observations than the 80% case. This relationship holds true for the 44% and 34% cases as well, as the 44% case produced 14% more observations, shown in Tbl. 2.

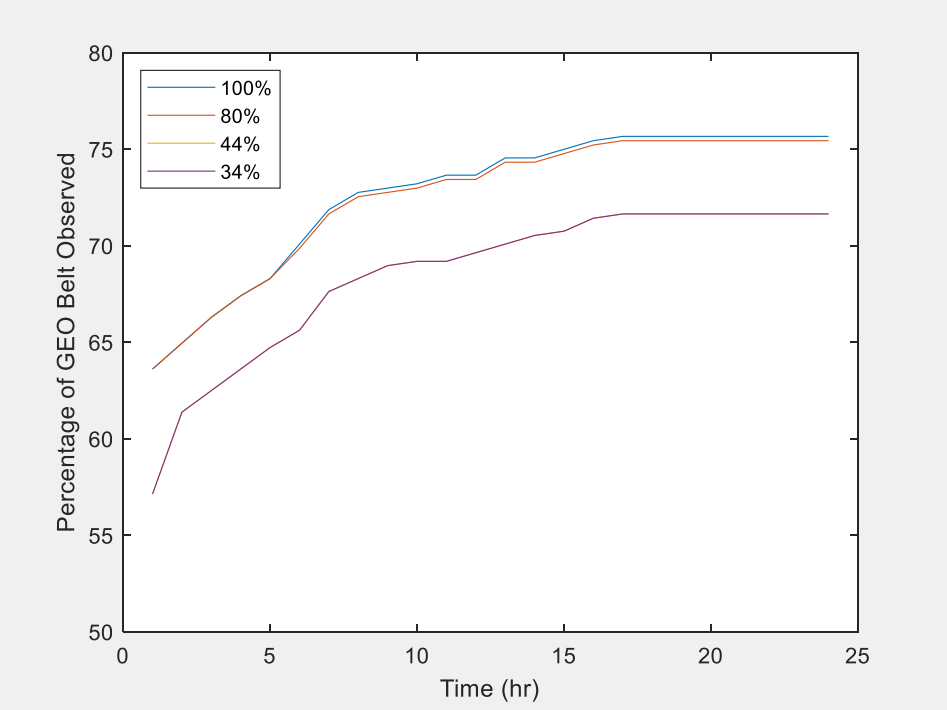

Fig. 14. Portion of Total RSOs Observed Over Time

Tbl. 2. Duty Cycle Summary

Duty Cycle (%)	Total # of Obs	RSOs in FoV	Detected RSOs	Time to Max Catalog Obs (hr)
100	96,925	399	338	17
80	84,169	398	337	17
44	53,344	378	320	17
34	45,697	378	320	17

Overall, the 44% and 34% duty cycle cases have more RSOs experiencing fewer revisits, while the 100% and 80% duty cycle cases have more RSOs that are more frequently revisited. The effect of the solar phase angle on RSO detection, specifically for the cases where polar coverage is available, is apparent in the number of RSOs observed 600 or more times. The same duty cycle cases yield different RSO observation characteristics at different seasons throughout the year, shown in Fig. 15, Fig. 16, and Fig. 17. The Vernal Equinox has the least favorable solar geometry, but a few RSOs are detected 600 times over 24 hours only for the 100% duty cycle case. The phase angles at the Winter Solstice enable a few RSOs to be detected 700 times for that same case. Finally, the Summer Solstice solar geometry facilitates RSOs to be revisited 600 and 700 times for both the 100% and 44% cases. This implies the solar phase angles at the poles enable many more revisits than normally expected for some RSOs. More specifically, the Sun's 23.5° inclination over the Equatorial plane at the Summer Solstice likely provides phase angles above, but still close to, 30° for the LEO satellites in the southern hemisphere.

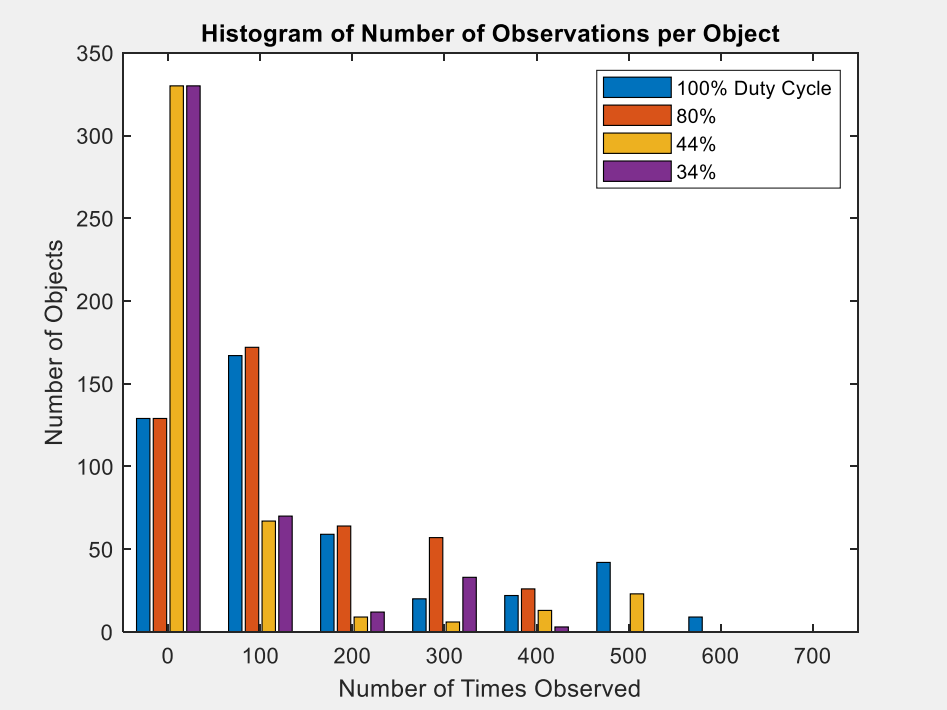

Fig. 15. RSO Observations for All Duty Cycles at Vernal Equinox

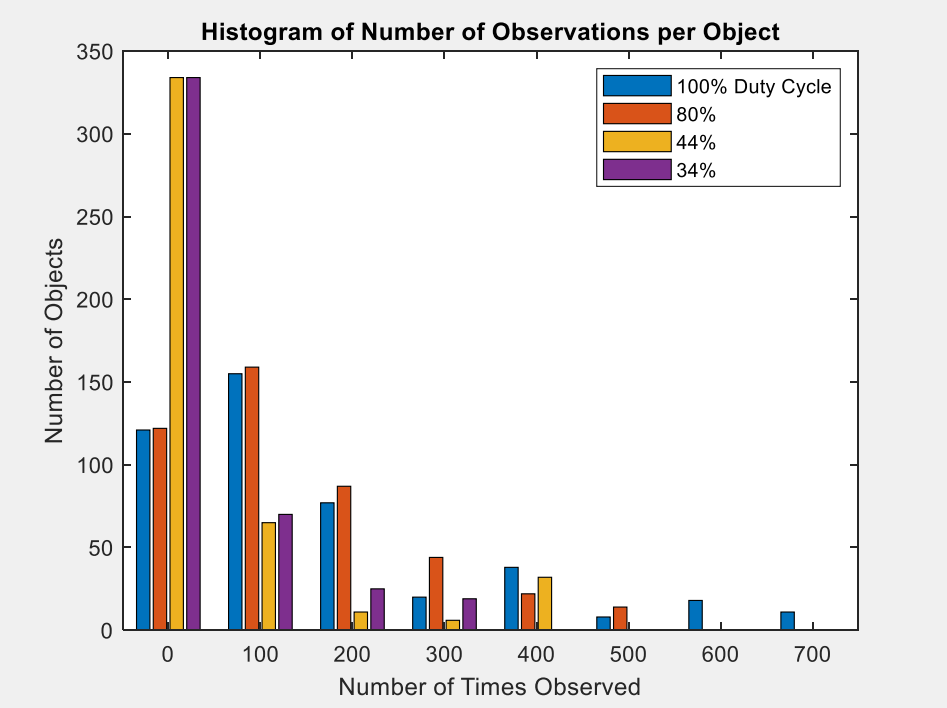

Fig. 16. RSO Observations for All Duty Cycles at Winter Solstice

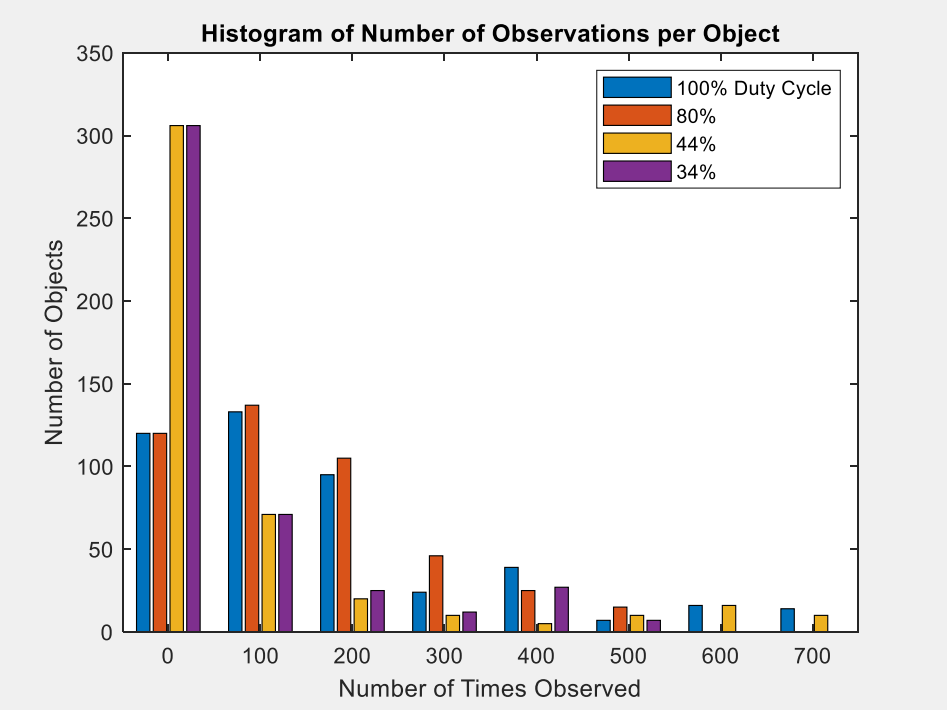

Fig. 17. RSO Observations for All Duty Cycles at Summer Solstice

4. CONSIDERATIONS FOR IMPROVING PERFORMANCE

Given the large number of mission vehicles in our model, all with nearly continuous line-of-sight access to the GEO belt, the large amount of observations in Tbl. 2 is expected. However, there are still several areas to address that can improve performance of both the sensors and the constellation. The best case revisit times show great opportunity to persistently monitor RSOs. The worst case revisit times even demonstrate that each detectable RSO can be seen on multiple instances within one day. A more sophisticated pointing scheme could aim the sensors to specific targets of interest and even provide stereo coverage.

The 44% duty cycle case produces many observations with sufficient revisit times to be considered a viable candidate for further evaluation and CONOPS development. The spacecraft could feature either a shared or individual sensor that is either body-fixed or gimbaled, and it can operate nearly any time if missile activity is mainly the Northern Hemisphere. The 17-hour observation latency merits a deeper investigation and could be due to a number of factors like our simulated sample rate or solar phase angle.

Two ways to mitigate performance degradation caused by solar phase angle, from a sensor perspective, are to increase the integration time and/or increase the aperture size. Increasing the integration time has limitations, where smearing of collected RSO signal across detectors should be avoided. If the sensor is operated in sidereal detection mode, the stars will remain still while targets streak across the FPA. This requires balancing the time of energy collection with the detector's instantaneous field of view (IFOV) and the relative velocity of the target RSO(s) [8]. Our modeled LEO sensor has an IFOV of 23.7 microradians, which allows an integration time up to 0.65 seconds before energy from one RSO is detected by multiple pixels. The curve in Fig. 18 represents the maximum desirable integration time for the sensor, given a design choice in IFOV.

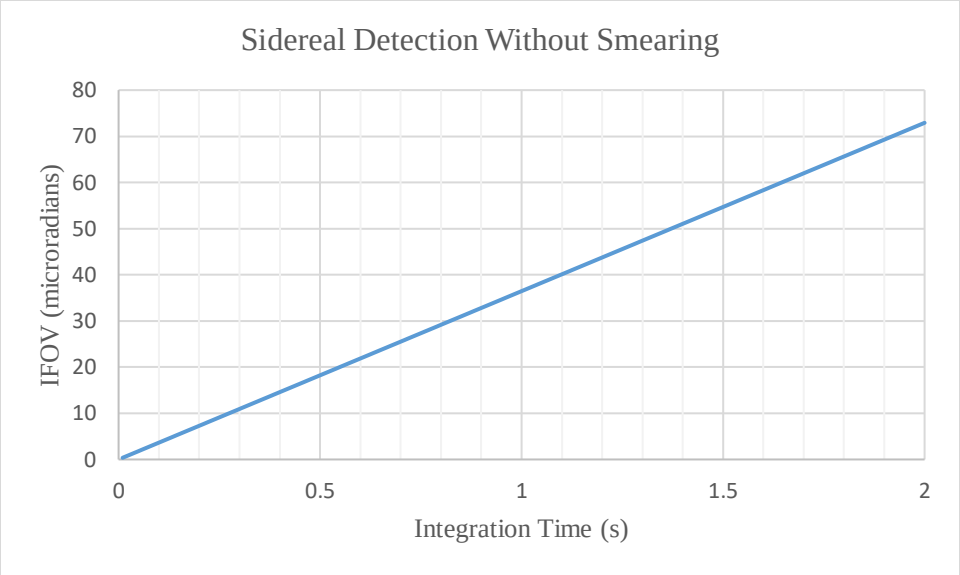

Fig. 18. Limits on Integration Time

Increasing the aperture size, assuming all other sensor design parameters are held constant, provides more energy to the FPA and each detector. This effectively provides more accurate observations and decreases the size of the MDT for every solar phase angle [9], shown in Fig. 19. Doubling the aperture size to 30 cm would improve the MDT from 110 cm to 55 cm at optimal solar geometry, enabling observation of more payloads and rocket bodies, however much debris is smaller than 50 cm [6]. There are obviously other cost, size, weight, and power challenges also to consider with a larger aperture. However, economies of scale may be leveraged for a proliferated system to drive down the cost per system.

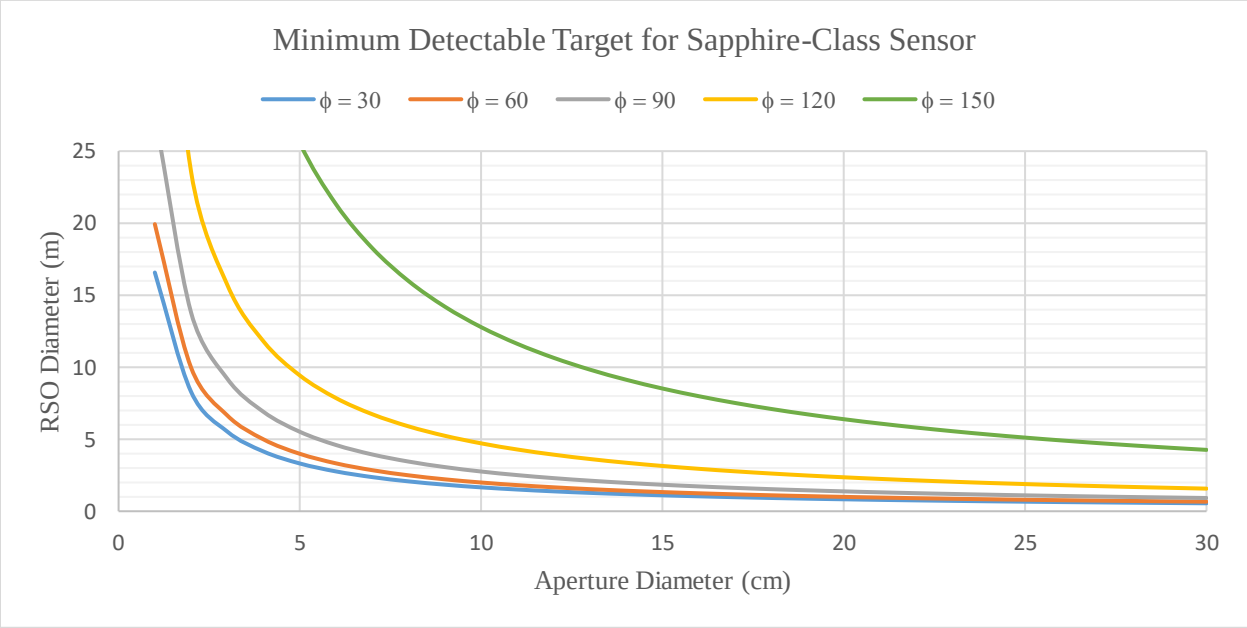

Fig. 19. Effects of Aperture Diameter on MDT, Over Various Solar Phase Angles

Tbl. 3. Effects of Aperture Diameter on MDT at Solar Phase Angle of 30°

Solar Phase Angle = 30°			
Aperture Diameter (cm)	**MDT Diameter (m)**	**Aperture Diameter (cm)**	**MDT Diameter (m)**
7	2.36	19	0.87
8	2.07	20	0.82
9	1.84	21	0.78
10	1.65	22	0.75
11	1.50	23	0.72
12	1.38	24	0.69
13	1.27	25	0.66
14	1.18	26	0.63
15	1.10	27	0.61
16	1.03	28	0.59
17	0.97	29	0.57
18	0.92	30	0.55

Increasing the sensor's overall sensitivity while balancing its resolution characteristics should also be considered when increasing aperture size. The Space Based Space Surveillance (SBSS) satellite in LEO has a 30 cm optical telescope for GEO RSO identification, which makes its sensor more sensitive than Sapphire's [3]. It also has larger pixels relative to its focal length, which provides a larger IFOV and biases the sensor more toward sensitivity than resolution. The 'Q' values for Sapphire and SBSS shown in Fig. 20 provide a relative comparison of their sensitivity. Q is the ratio of the sensor's operating wavelength to the product of its aperture diameter and IFOV. One potential advantage of increasing IFOV is the opportunity to increase integration time while avoiding smearing energy across pixels.

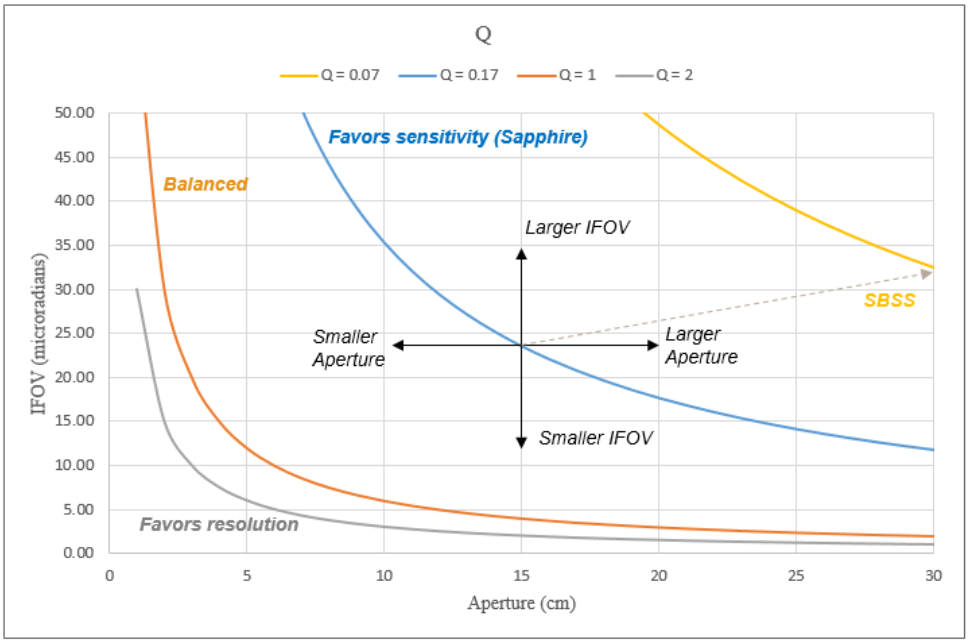

Fig. 20. Sensitivity vs. Resolution for Sapphire and SBSS

5. UTILITY OF THE SECONDARY MISSION

The second main objective of this study is to determine the effectiveness of the secondary mission in improving the accuracy of orbit determination for GEO RSOs. The contribution of the secondary mission was first analyzed on its own, independent of any other tracking system. Results were then compared with results from GEODSS, and then both systems were analyzed in conjunction to determine the value added.

Orbit determination was performed using the extended Kalman filter (EKF) in Orbit Determination Toolkit (ODTK) on a typical RSO, EchoStar 105. To establish a baseline performance, observations from the SSN were simulated using the included tracking data simulator. Tracking stations used in this analysis were the 3 GEODSS sites at Socorro, NM, Maui, HI, and Diego Garcia, in addition to the Millstone Hill and Globus II deep space tracking radars. Estimation of tracker biases was not considered in this analysis. It was assumed that biases were already well-characterized. Seven states were estimated by the filter, including position x, y, z, velocity x, y, z, and solar radiation pressure.

Using the methodology, tools, and constraints outlined in Vallado [10], a realistic tracking schedule was generated for each SSN site and loaded into the simulator in ODTK. Observations were then generated for a 24 hour period. These observations were then run through the EKF and results were analyzed. The primary figure of merit was the resulting position uncertainty shown in Fig. 21.

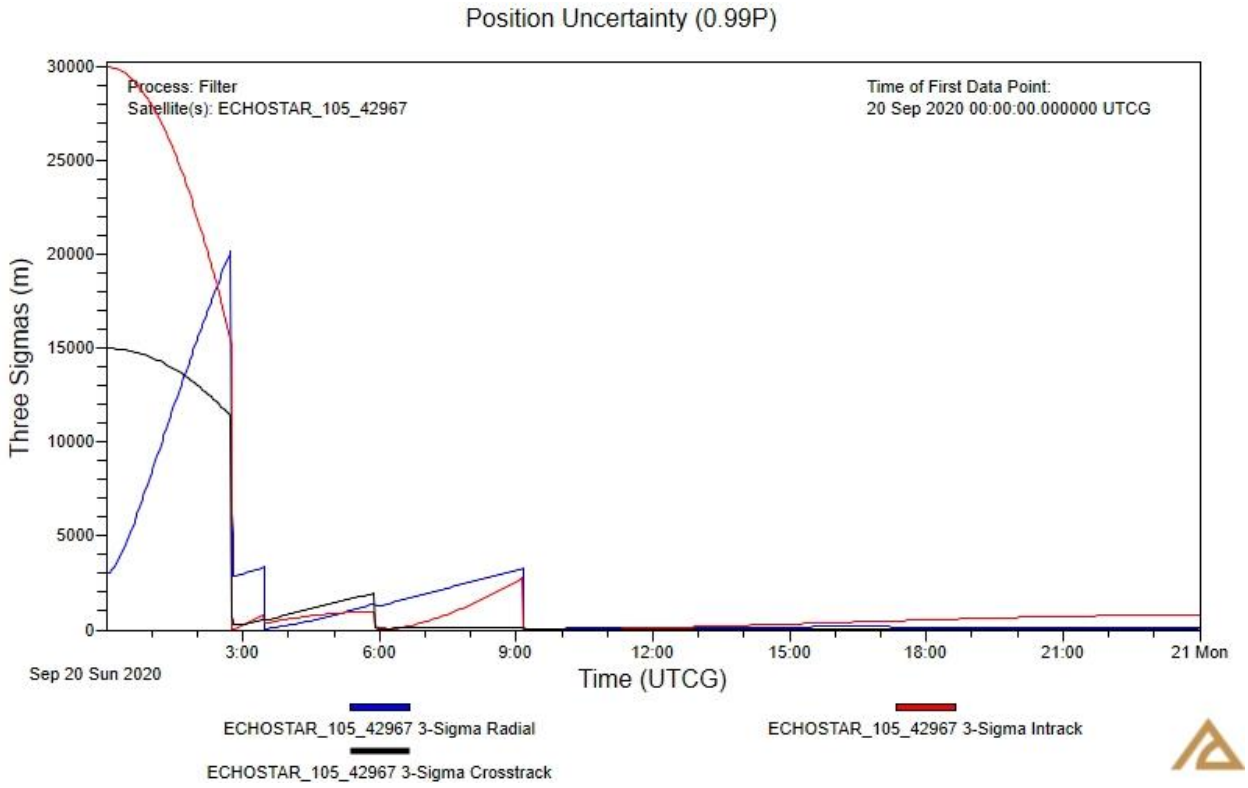

Fig. 21. Position Uncertainty (3-Sigma) – SSN Baseline

The filter takes nearly 3 hours to converge, shown in Fig. 21. Fairly good results are achieved at a little over 9 hours, but the uncertainty then grows for the remainder of the 24 hours as the system is starved for data. Performance is decent for the very limited number of observations, in this case 3 optical tracks containing right ascension/declination pairs from Socorro and Maui, and one radar track from GlobusII with range, azimuth, and elevation data. At the end of 24 hours, position uncertainty was 102.5 m radial, 820.1 m in-track, and 19.8 m cross-track.

Tracking intervals for the secondary mission were generated using STK, applying realistic constraints and calculating access. Access was limited to times where the target was illuminated by the sun, either in direct sun or penumbra. Solar phase angle was constrained to a range from 30° - 150°. Solar and lunar exclusion angles were applied at 30° and 10°, respectively. Minimum access duration was set to 1 second, corresponding to the total integration time on the sensor (10 coadds at 0.1 sec integration time each). With these constraints enforced, constellation access to the target satellites was calculated, and an interval file was produced containing the tracking intervals. The CONOPS implemented for this study corresponds to the 44% duty cycle described above, where the secondary mission is performed only when the spacecraft is below 10° south latitude, and the spacecraft sensor is pointed at the GEO belt at the longitude of the host spacecraft. The longitude rate does increase to approximately 0.11 deg/sec as the spacecraft reaches its lower latitude limit, but the targeting algorithm and sensor processing can compensate for the high rate.

Tracking intervals from STK were loaded into the tracking data simulator as custom tracking intervals and observations were generated for the constellation. These observations were again run through the EKF as before, and results analyzed. The resulting position uncertainty is shown in Fig. 22.

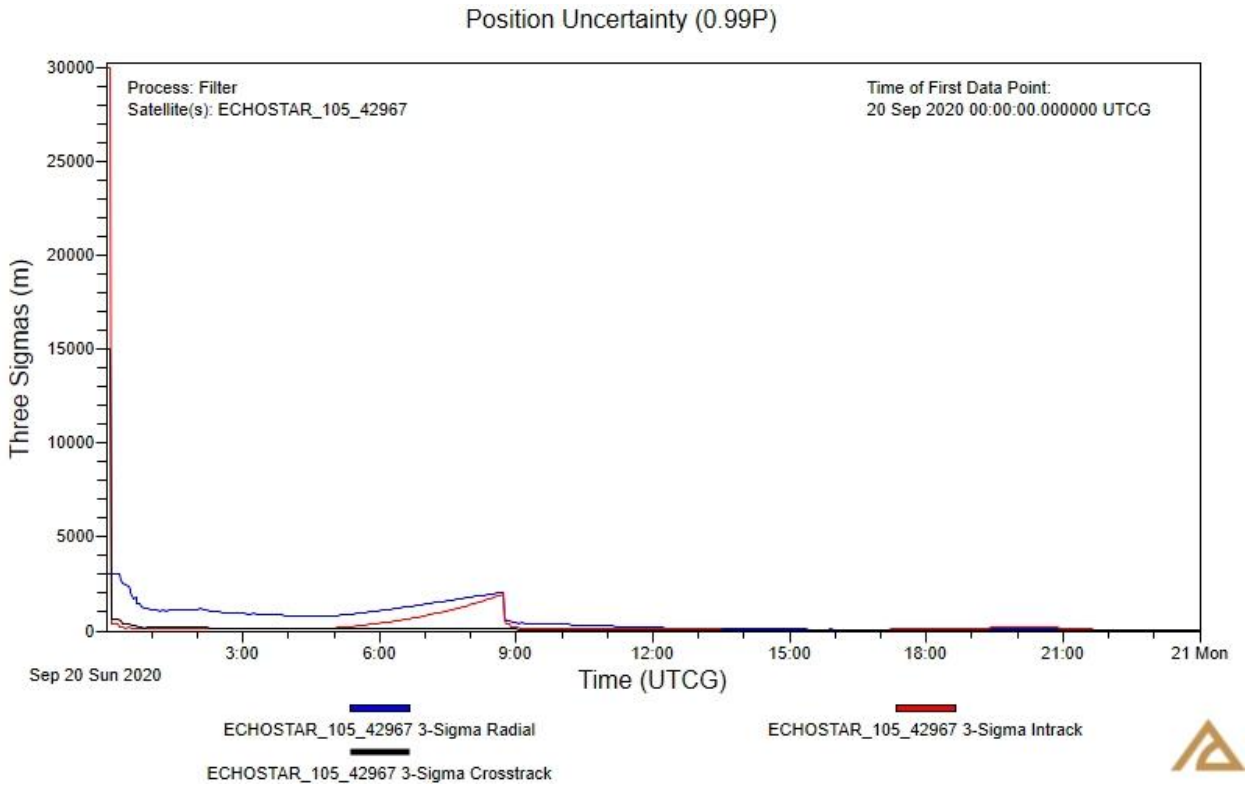

Fig. 22. Position Uncertainty (3-sigma), SSA Constellation Alone

In this case the filter converges just over 9 minutes into the scenario, and uncertainties in all 3 axes, radial, in-track, and cross-track (RIC), fall to less than 1 km only 6 hours in. The two areas of growth in uncertainty from approximately 6:00 – 8:30, and again from approximately 18:00 – 21:00 correspond to times where the solar phase angle is unfavorable and therefore there is no tracking data. The position uncertainty at the end of 24 hours is 55.6 m radial, 60.7 m in-track, and 23.7 m cross-track. Ample observations from multiple observers over the entire 24 hour analysis period produces excellent results.

The EKF was then run again to process all of the observations from both the ground and space-based trackers simultaneously. Position uncertainty results are shown in Fig. 23.

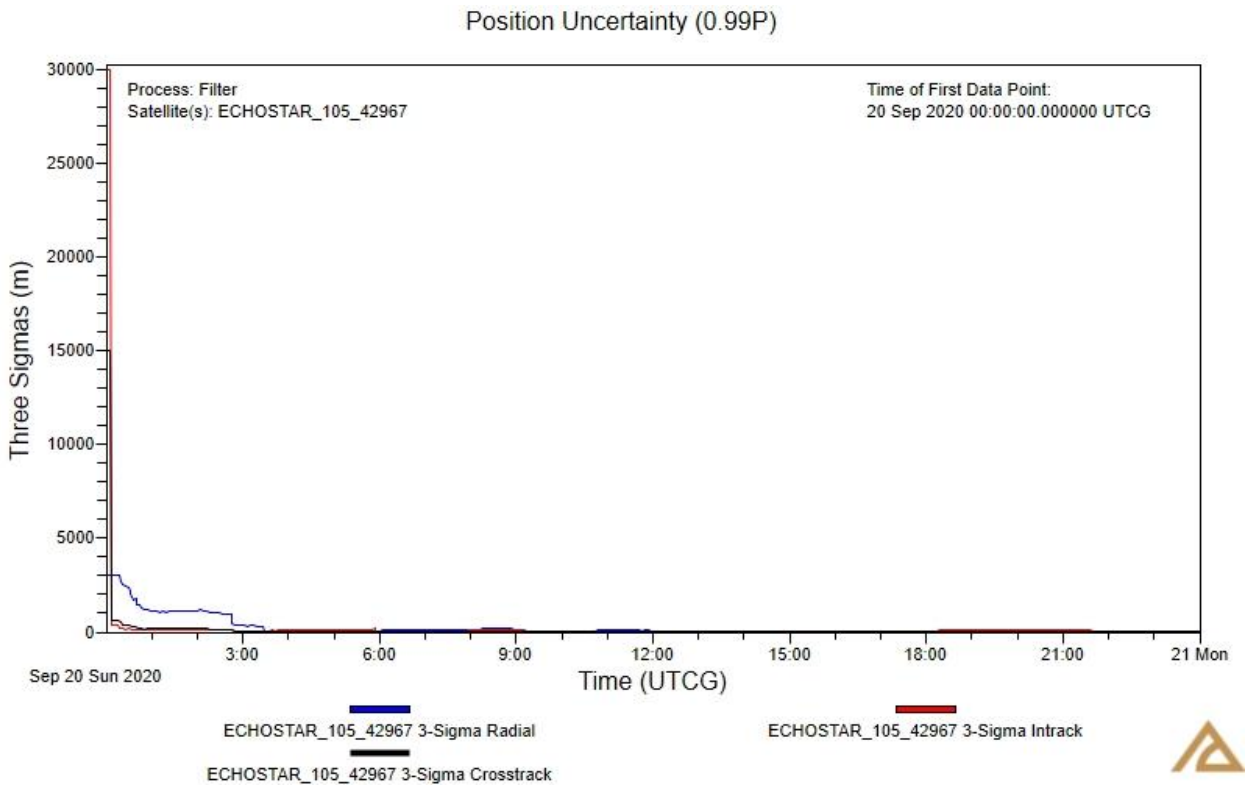

Fig. 23. Position Uncertainty (3-sigma) – SSN and Space-Based Tracking Combined

With combined tracking, the filter quickly converges, and the supplemental tracking from the ground has somewhat removed the slight rises in uncertainty during the unfavorable solar phase angle periods. Position uncertainty with combined tracking at the end of the 24 hour analysis interval was further reduced to 49.6 m radial, 58.8 m in-track, and 14.8 m cross-track.

The value of augmenting existing, ground-based tracking systems with space-based tracking is clearly evident. There is a 51.6% improvement in radial position uncertainty, a 92.8% improvement in in-track position uncertainty, and a 25.2% improvement in cross-track position uncertainty over ground-based tracking alone. It is expected that performance will be similar with other RSOs as the target. The large number of observations from multiple, widely dispersed observers throughout the tracking period results in better and more consistent custody of the observed RSOs. While not specifically analyzed here, it is expected that maneuver detection, characterization, and recovery will be improved significantly in speed and accuracy. The probability that a maneuver will occur during a short and infrequent SSN pass is very low, and if a maneuver occurs, it can be days before it is detected, let alone characterized, and even longer before custody is restored. Near continuous coverage with space-based tracking will shorten this to hours or less. Convergence on a viable solution is also much faster (95% faster in this case), the quality of the solution is much improved, and that quality is easily maintained going forward.

The addition of a secondary SSA mission to the proposed Tracking Layer or other LEO constellations can be done at significant cost savings over a dedicated SSA constellation. Whether that system makes use of the primary mission sensor during primary mission downtime, or a secondary, steerable sensor payload is mounted on the zenith surface of the spacecraft and shares optical path and processing with the primary mission, it still results in a very effective SSA system at less expense.

6. CONCLUSIONS & FUTURE WORK

We have outlined a modeling and simulation approach to evaluate the utility of a large-scale GEO space surveillance mission from LEO. More specifically, we show that hosting a secondary SSA mission on a pLEO missile warning and tracking constellation can enhance the SSN's layered architecture. The concept provides more volume and diversity of observations, quicker revisit rates, more metric tracks, better object custody, and improved safety of flight through more accurate orbit determination. Considerations for follow-on studies include evaluating the utility of an SSA sensor for ballistic missile tracking. Results could determine if the sensor can be shared or dedicated to the secondary mission. A study characterizing the effectiveness of the LEO system on maneuver detection, characterization, and recovery would also be useful. Other mission modeling aspects to investigate are alternate sensor pointing schemes, sensor models, and space architectures. A parametric analysis of constellation size could also reveal similar utility with a smaller set of satellites. Leveraging this approach can help shape future space architectures and mission designs, ultimately improving space domain awareness at reduced costs to the SSA community.

7. ACKNOWLEDGEMENTS

Thanks to John Bloomer and Darin Koblick of Raytheon Intelligence and Space for lending their overall support for this project along with their physics-based sensor and mission expertise. Doug Cather and Dave Vallado of AGI also provided invaluable technical advice and analytical tool support.

8. REFERENCES

[1] *National Defense Space Architecture (NDSA), Systems, Technologies, and Emerging Capabilities (STEC),* Space Development Agency, 2020.

[2] R. Zmarzlak, *Missile Tracking Satellites Explore New Missions,* Advantech Wireless, 2013.

[3] M. R. Ackerman, R. R. Kiziah, P. C. Zimmer, J. T. McGraw and D. D. Cox, *A Systematic Examinaiton of Ground-Based and Space-Based Approaches to Opitcal Detection and Tracking of Satellites,* 31st Space Symposium, 2015.

[4] *CCD47-20 Back Illuminated High Performance AIMO Back Illuminated CCD Sensor,* e2v technologies, 2006.

[5] H. Yura, *Threshold Detection in the Presence of Atmospheric Turbulence,* Applied Optics, 1995.

[6] D. C. Koblick, P. Shankar and S. Xu, *Publicly Available Geosynchronous (GEO) Space Object Catalog for Future Space Situational Awareness (SSA) Studies,* Advanced Maui Optical and Space Surveillance Technologies Conference, 2017.

[7] M. D. Hejduk, *Specular and Diffuse Components in Spherical Satellite Photometric Modeling,* Advanced Maui Optical and Space Surveillance Technologies Conference, 2011.

[8] M. D. Hejduk, J. V. Lambert, C. M. Williams and R. L. Lambour, *Satellite Detectability Modeling for Optical Sensors.*

[9] J. R. Schott, Remote Sensing: The Image Chain Approach, Oxford University Press, 2007.

[10] D. A. Vallado and J. D. Griesbach, *Simulating Space Surveillance Networks*, Girdwood: American Astronautical Society / American Institute of Aeronautics and Astronautics, 2011.